Complex transient dynamics of stage-structured sopulations in response to environmental changes

Massie, Thomas M ; Ryabov, Alexei ; Blasius, Bernd ; Weithoff, Guntram ; Gaedke, Ursula

Abstract: Stage structures of populations can have a profound influence on their dynamics. However, not much is known about the transient dynamics that follow a disturbance in such systems. Here we combined chemostat experiments with dynamical modeling to study the response of the phytoplankton species Chlorella vulgaris to press perturbations. From an initially stable steady state, we altered either the concentration or dilution rate of a growth-limiting resource. This disturbance induced a complex transient response—characterized by the possible onset of oscillations—before population numbers relaxed to a new steady state. Thus, cell numbers could initially change in the opposite direction of the long-term change. We present quantitative indexes to characterize the transients and to show that the dynamic response is dependent on the degree of synchronization among life stages, which itself depends on the state of the population before perturbation. That is, we show how identical future steady states can be approached via different transients depending on the initial population structure. Our experimental results are supported by a size-structured model that accounts for interplay between cell-cycle and population-level processes and that includes resource-dependent variability in cell size. Our results should be relevant to other populations with a stage structure including organisms of higher order.

DOI: https://doi.org/10.1086/670590

Complex Transient Dynamics of Stage-Structured Populations in Response to Environmental Changes.

Author(s): Thomas M. Massie, Alexei Ryabov, Bernd Blasius, Guntram Weithoff, and Ursula Gaedke

Source: *The American Naturalist*, Vol. 182, No. 1 (July 2013), pp. 103-119
Published by: The University of Chicago Press for The American Society of Naturalists
Stable URL: http://www.jstor.org/stable/10.1086/670590
Accessed: 19/09/2013 04:36

Complex Transient Dynamics of Stage-Structured Populations in Response to Environmental Changes

Thomas M. Massie,[1,2,*,†] Alexei Ryabov,[3] Bernd Blasius,[3] Guntram Weithoff,[1] and Ursula Gaedke[1]

1. Department of Ecology and Ecosystem Modeling, University of Potsdam, Maulbeerallee 2, 14469 Potsdam, Germany; 2. Institute of Evolutionary Biology and Environmental Sciences, University of Zurich, Winterthurerstrasse 190, 8057 Zurich, Switzerland; 3. Institute for Chemistry and Biology of the Marine Environment (ICBM), Carl-von-Ossietzky University of Oldenburg, Carl-von-Ossietzky-Straße 9-11, 26111 Oldenburg, Germany

Submitted January 12, 2012; Accepted February 6, 2013; Electronically published June 5, 2013

Online enhancements: appendixes, supplementary figures. *Dryad data:* http://dx.doi.org/10.5061/dryad.bb5t3.

ABSTRACT: Stage structures of populations can have a profound influence on their dynamics. However, not much is known about the transient dynamics that follow a disturbance in such systems. Here we combined chemostat experiments with dynamical modeling to study the response of the phytoplankton species *Chlorella vulgaris* to press perturbations. From an initially stable steady state, we altered either the concentration or dilution rate of a growth-limiting resource. This disturbance induced a complex transient response—characterized by the possible onset of oscillations—before population numbers relaxed to a new steady state. Thus, cell numbers could initially change in the opposite direction of the long-term change. We present quantitative indexes to characterize the transients and to show that the dynamic response is dependent on the degree of synchronization among life stages, which itself depends on the state of the population before perturbation. That is, we show how identical future steady states can be approached via different transients depending on the initial population structure. Our experimental results are supported by a size-structured model that accounts for interplay between cell-cycle and population-level processes and that includes resource-dependent variability in cell size. Our results should be relevant to other populations with a stage structure including organisms of higher order.

Keywords: chemostat experiments, *Chlorella vulgaris*, environmental changes, population dynamics, stage structure, transient dynamics.

Introduction

The dynamics of populations and communities are determined by the interplay between their internal structure and external conditions. While the study of environmental influences on long-term attracting states has a long history in ecology, determining the transient response of a population to changes in environmental conditions remains a central challenge (Haddad et al. 2002; Coulson et al. 2004; Cattadori et al. 2005; Jenouvrier et al. 2005; Manderson 2008). Transient dynamics can be defined as "behavior that is different from the long-term behavior" (Hastings 2004). It reflects a dynamic transition between two population-dynamical steady states induced by a change in or perturbation of environmental conditions. The resulting transients can be highly complex, may vary on different temporal scales, and are frequently observed in natural time series (Bierzychudek 1999; Clutton-Brock and Coulson 2002; Coulson et al. 2004).

Complex transient dynamics is of particular importance in stage-structured populations because different developmental stages may interact differently with the environment. Therefore, an organism's life cycle, including all stages of ontogenetic development, directly determines the dynamic response of a population to a perturbation (e.g., a sequoia is likely to respond on a broader timescale than a mayfly would). By influencing the biology and life cycle of individual organisms, environmental changes affect the dynamics of entire populations (Walther et al. 2002; Parmesan and Yohe 2003). Predicting the response of a stage-structured population to environmental changes requires an understanding of the mechanisms by which the different developmental stages are influenced. The number of such mechanisms increases significantly when stage-dependent interactions are relevant and when they may either stabilize or destabilize population dynamics (Tuljapurkar and Caswell 1997; Caswell 2000; Radchuk et al. 2012).

One remarkable phenomenon of structured populations is the occurrence of oscillations (Kendall et al. 1999; Caswell 2000; Mueller and Joshi 2000). Oscillations in pop-

* Corresponding author. Present address: Institute of Evolutionary Biology and Environmental Sciences, University of Zurich, Winterthurerstrasse 190, 8057 Zurich, Switzerland; e-mail: thomas.massie@ieu.uzh.ch.

† T. M. Massie, G. Weithoff, U. Gaedke, and B. Blasius designed the research; Massie and Weithoff performed the experiments; Blasius, A. Ryabov, and Massie formulated the mathematical model; Massie, Ryabov, and Blasius analyzed the data; and Massie, Gaedke, Ryabov, and Blasius wrote the article.

Am. Nat. 2013. Vol. 182, pp. 103–119.
DOI: 10.1086/670590

ulation numbers are often caused by multispecies interactions (e.g., predator-prey or host-parasite relations), but they can also occur in single-species systems due to inherent demographic properties. At steady state, a population has a characteristic stage distribution reflecting adjustment to the prevailing environmental conditions influencing the single stages, for example, the proportion of juveniles whose survival is temperature dependent. If this distribution is perturbed, a cohort of individuals that have shared a particular experience during a particular life stage is formed. Generally, this is tantamount to the synchronization of a population: the higher the degree of synchronization, the higher the contribution of the cohort to the whole population. If the vast majority of individuals grows, reproduces, and dies at the same time, a population starts to oscillate.

The occurrence of complex dynamic behavior resulting from stage structure has most impressively been demonstrated in populations of flour beetles (*Tribolium* sp.; Costantino et al. 1995; Henson et al. 1998; Dennis et al. 2001). These holometabolic insects have well-defined and morphologically distinguishable life stages (egg, larva, pupa, and imago) with distinct characteristics that certainly structure a population. On the contrary, the developmental stages of a vast number of species cannot be clearly associated with distinct morphological shapes but rather appear as phases that differ only in physiology or behavior. This type of population structure is exhibited by even simple, unicellular microorganisms (Balagaddé et al. 2005; Hatzis and Porro 2006; Cipollina et al. 2007; Massie et al. 2010) and arises from physiologically distinct phases within the cell cycle (Vaulot et al. 1987; Arino and Kimmel 1993; Pascual and Caswell 1997).

A typical example of a unicellular microorganism with this type of structure is the phytoplankton species *Chlorella vulgaris*, which possesses a eukaryotic cell cycle with four physiologically distinct stages (the G_1, S, G_2, and M phases). The life cycle of a newly released daughter cell begins in the G_1 phase. When a critical amount of essential nutrients and biochemical compounds such as proteins have been accumulated, the cell enters the next stage (Morgan 2007; Humphrey and Brooks 2010). In this S phase, DNA is synthesized and replicated. In the following G_2 phase, the cell arranges everything to allow for cell division in the M phase. In this last phase, the cell enters mitosis and finally releases daughter cells (typically, four). The cell cycle is controlled by the internal concentration of essential nutrients. A lack of nitrogen in the G_1 phase stops the transition into the S phase (Gould et al. 1981; Olson and Chisholm 1986; Olson et al. 1986; Vaulot et al. 1987) and prevents a cell from starting DNA synthesis, which otherwise would not be successful. That is, cell progression inside the G_1 phase is nitrogen dependent, while the progression velocity for all other stages is nitrogen independent. Hence, nitrogen-sensitive development in the G_1 phase of the cell cycle is a simple but effective mechanism generating a dynamic population structure based on the availability of nitrogen in the surrounding medium. This makes *C. vulgaris* an interesting and easily culturable model organism for studying the interplay between population dynamics and external conditions.

In this study, we combined laboratory experiments with mathematical modeling to investigate both the demographic and dynamical responses of the physiologically structured algal population *C. vulgaris* to permanent changes in its environmental conditions. We imposed press perturbations by altering either the dilution rate, δ, or the supply concentration of the growth-limiting resource, N_i. In this way, we directly changed the environmental conditions to observe the impacts on population dynamics. This distinguishes our study from many others in which the population structure was directly manipulated via "selective harvesting," that is, by reducing the number of individuals belonging to a specific developmental stage (Costantino et al. 1995; Benton et al. 2004; Cameron and Benton 2004). In a previous study, Massie et al. (2010) synchronized *C. vulgaris* populations in a chemostat by turning off the dilution process for several days. Once synchronized by this pulse perturbation, the populations exhibited cyclic behavior, with periods defined by generation time. However, such a harsh "off-on" manipulation is rather uncommon in natural systems. In contrast, here we applied press perturbations of δ that lasted throughout our experiments. We expected the transient dynamics to be dependent on the direction of the change as well as the intensity and absolute values of δ before and after the perturbation. We applied environmental perturbations by (1) doubling the concentration of the limiting resource in the supply medium N_i and (2) increasing or decreasing δ. A doubling of N_i allowed us to investigate the dynamic behavior that results from an ameliorated resource availability, for example, resource enrichment or eutrophication in aquatic systems due to global change (Quayle et al. 2002; Jeppesen et al. 2007). Since the amounts of resources entering the system per unit time and algal mortality are interdependent, varying δ imposed changes on the system's turnover rate. Thus, we were able to address the effects of permanently altering resource limitation on population dynamics.

We obtained estimates of population abundance every 5 min. This unusually frequent sampling of time series helped to identify dynamics unlikely to be detected by 12- or 24-h sampling intervals. Particle counter measurements of size distributions as well as data on cell number P, total population biovolume V_B, and mean cell volume V_C were taken every 4–8 h. These size-distribution measurements

allowed us to track cell-size variability according to developmental stages, from small daughter cells to large mother cells.

Interpretation of our experimental results is supported by a mathematical model based on a stage-structured model developed by Massie et al. (2010). That model divides the life cycle of phytoplankton cells into two stages: a first stage (the G_1 phase), where progression through the cell cycle is nitrogen dependent, and a second stage (composed of the S, G_2, and M phases), where it is not. This leads to the onset of synchronization of the two life stages due to nitrogen limitation and is reflected by the emergence of sustained oscillations in cell density and population structure (Massie et al. 2010). To realistically describe the transient dynamics, we extended this model with an additional mechanism that captures plastic adaptations of the cell cycle to varying nitrogen concentrations such that the size of a cell varies not only within the developmental stages but also in response to the availability of nitrogen. That is, we assume that the nitrogen concentration has an influence on the duration of the G_1 phase, allowing the algal cells to grow larger at high nitrogen concentrations (Caperon and Meyer 1972; Rhee 1978). This model extension accounts for the fact that under nonlimiting conditions, cells in the G_1 phase can take up surplus nitrogen (in excess of the minimum requirements for reproduction) to synthesize higher amounts of cell compounds like amino acids or proteins (Rhee 1978; Dortch et al. 1984). Hence, the cells grow larger compared to cells under strongly limiting concentrations. Our numerical simulations reveal that the combination of both mechanisms, namely synchronization due to nitrogen limitation and nitrogen-related cell-size variability, can provoke highly complex population-level responses to changes in environmental parameters.

Our study shows that microbial populations may exhibit complex transient dynamics in response to press perturbations of the environment that are directly assigned to the structure of a population. In particular, we found that this complex transient response was characterized by the possible onset of oscillations before the population numbers relaxed to a new steady state. Thus, we observed a counterintuitive behavior in which cell numbers initially changed in the opposite direction of the long-term change. In particular, a sudden increase in nitrogen resulted in a transient decrease in cell numbers. Furthermore, the response depended on both the way in which the environmental parameters changed and the population's initial stage structure. That is, identical future steady states were approached via different transients depending on the initial population structure. To characterize the transients, we present several quantitative indexes that measure their return rate to equilibrium, duration, amplitude, and reactivity. The experimental data agree with predictions obtained from our mathematical model, suggesting that we have identified the critical mechanisms and processes leading to the observed dynamics.

Methods

Chemostat Setup

We established monoclonal batch cultures of the green algae *Chlorella vulgaris* (Chlorococcales) and kept them in a climate chamber at 23.3° ± 0.4°C under a constant fluorescent illumination of 110 $\mu E \cdot m^{-2} \cdot s^{-1}$ (to prevent synchronization by light-dark cycles). The batch cultures served as stock cultures for the chemostat experiments. Nitrogen concentrations were adjusted to be nonlimiting or only weakly limiting. We used a sterile, modified WC Woods Hole medium following Guillard and Lorenzen (1972; pH = 6.8). The nitrogen concentration of the supply medium N_i was set to 80 $\mu mol \cdot L^{-1}$, low enough to limit algal growth. The medium contained trace metals, vitamins, and other nutrients in nonlimiting concentrations. For stock cultures, we used medium containing 320 μmol nitrogen per liter. We used 1.5-L glass chemostat vessels and adjusted the culture volume to approximately 800 mL. To provide homogeneous mixing and to prevent CO_2 limitation, algal cultures were bubbled with sterile air.

We measured cell number P, total population biovolume V_B, and mean cell volume V_C using a CASY (Innovatis) particle counter. Light-extinction measures serve as an accurate proxy for V_B (Massie et al. 2010). Following Walz et al. (1997), we measured light extinction as light transmittance (wavelength $\lambda = 880$ nm) through a sterile syringe that pulled out and pushed back 10 mL of chemostat content every 5 min. This quasi-continuous, noninvasive method provided the high temporal resolution necessary to analyze population dynamics in detail. Algal growth on the wall of the syringe was prevented due to the bidirectional movement of the syringe plunger. The measurement devices were connected to a computer that automatically stored the data.

Experimental Design

To test for the responses of populations to changing environmental conditions, we imposed press perturbations by separately altering the two fundamental parameters defining a chemostat system: (1) the resource influx into the system, represented by the nitrogen concentration of the supply medium N_i, and (2) the system's turnover rate, represented by its dilution rate δ.

1. The system's resource influx was increased by doubling N_i from 80 to 160 $\mu mol \cdot L^{-1}$, while δ was kept con-

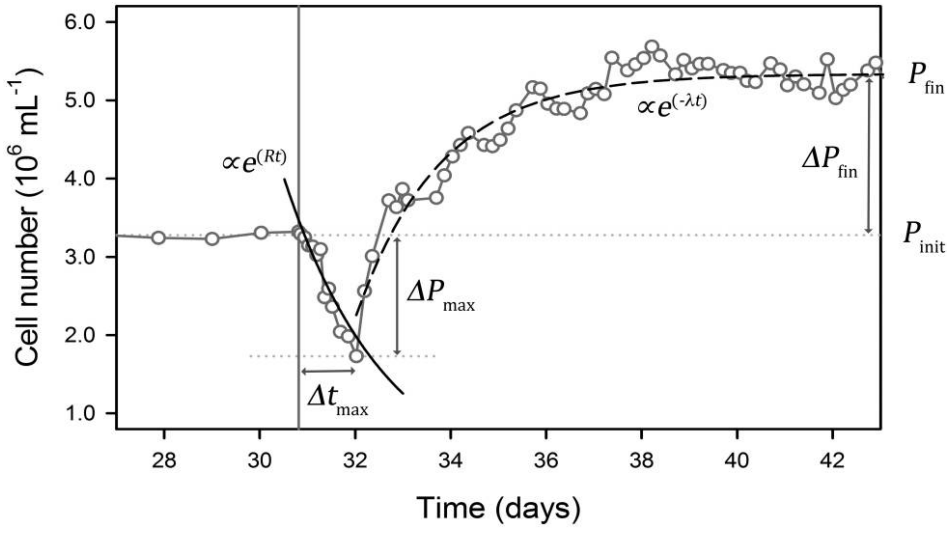

Figure 1: Schematic illustration of transient response indexes showing a typical time course of measured cell numbers $P(t)$ following a press perturbation. Data for cell numbers (circles) were taken from trial 3 ($\delta = 0.82$ day^{-1}); the vertical gray line at $t = 30.8$ days indicates the time instance of the disturbance when N_i was changed from 80 to 160 μmol · L^{-1}. The response of the population is characterized by two dynamic phases: an initial separation from the steady state P_{init}, followed by a relaxation to a new equilibrium P_{fin}. The solid black line indicates a least squares fit of the exponential function e^{Rt} to the initial population response. This defines the reactivity R as the per capita changing rate immediately following the perturbation. Here R is negative because the cell numbers initially decay in response to the perturbation. The second phase of the transient is characterized by the return rate to the new equilibrium λ, which is obtained by an exponential fit $e^{-\lambda t}$ to the deviation $P(t) - P_{fin}$ (dashed black line). See online appendix A for a more detailed explanation.

stant at 0.48 day^{-1} (trial 1) and 0.82 day^{-1} (trial 2), respectively. This is qualitatively different from applying a single temporary addition of nutrients. Here the medium dripped into the chemostat vessel according to the value of δ. That is, the surplus of nitrogen entered the system not at once but gradually over time. With our setup, we addressed the response of natural populations to resource enrichment, such as eutrophication.

2. The system's turnover was altered by manipulating δ from 0.21 to 0.51 day^{-1} (trial 3), from 0.50 to 0.79 day^{-1} (trial 4), and from 0.82 to 0.51 day^{-1} (trial 5). Populations experienced a higher mortality when δ was increased. Additionally, increasing δ led to an ameliorated per capita nutrient availability, both directly, as the inflow of nutrient-containing medium per unit time was higher, and indirectly, as increasing washout reduced cell density, giving a single cell comparably more nutrients to grow on. As a result, cells remaining inside the chemostat vessel experienced better growth conditions, and the growth rate of the population increased, too, since $r = \delta$ at steady state. The opposite held for a reduction of δ.

Each time we started a chemostat experiment, we first inoculated *C. vulgaris* at very low densities (25,000–50,000 cells · mL^{-1}) and let the cultures grow until they reached steady state or were comparatively close to it. Prior to each perturbation, the chemostat populations were kept at this state for at least 5 days to ensure that all population-characterizing variables (P, V_B, V_C, and size distributions) showed no or only minor fluctuations.

Transient Response Indexes

Following Neubert and Caswell (1997), we used quantitative indexes to characterize the transient response to a disturbance (see fig. 1 and app. A; apps. A and B available online). The transient constitutes a change in population numbers from an initial steady state P_{init} to a final state P_{fin} and can be typically distinguished into two phases. The first phase corresponds to the direct population response immediately after the perturbation. During this phase, cell numbers change approximately exponentially in time, which is described by the reactivity R, or the per capita rate of change following the perturbation (obtained by a least squares fit of the measured time series to an exponential function). Note that this first response can be diametrically opposite to the final change in the population density, giving rise to a maximal deviation ΔP_{max} of population numbers from the initial state at some intermediate time interval Δt_{max} after the perturbation. The second phase of the transient describes the relaxation of the population to the new steady state. This phase can be characterized by the return rate to equilibrium λ as the rate

of exponential decay toward the new equilibrium. To standardize these measures, we use the relative numbers $\Delta P_{max}/P_{init}$ and $\Delta P_{fin}/P_{init}$ to quantify the transient and final amplitudes of the dynamic response, respectively.

Model Description and Parameter Fitting

We used numerical modeling to support our experimental findings and to explain the interplay between cell growth, stage structure, and population dynamics. The model is an extension of the size- and stage-structured chemostat model recently presented by Massie et al. (2010). In the model, the age of a cell is described by the phase variable θ, which can be interpreted as the cell's development index, or its position along the cell cycle. For each cell, θ advances according to its maturation velocity $g(N, \theta)$, with N being the nutrient concentration of the surrounding medium. Thereby, the cell cycle is subdivided into two basic stages: the G_1 phase $[\theta_0, \theta_c]$, in which $g(N)$ is nitrogen dependent, and the rest of the cycle (comprising the S, G_2, and M phases), in which g is constant,

$$g = g(\theta, N) = \begin{cases} \omega \dfrac{N}{K_N + N}, & \text{if } \theta \in [\theta_0, \theta_c] \\ \omega, & \text{otherwise.} \end{cases} \tag{1}$$

Here K_N is the half-saturation constant, and ω is the maximal maturation velocity. Within the G_1 interval, aging depends on the nitrogen concentration in a Monod-wise function; it becomes zero when the nitrogen concentration is exploited ($N = 0$), which ultimately causes the cells to cease developmental progression.

The new aspect of our model is that it allows the length of the G_1 phase to vary with the nutrient level. At high nutrient concentrations, the length of this phase increases, causing the cells to take up surplus nitrogen and to grow larger in size (see schematic representation in app. B). Thereby, the length of the G_1 phase is modeled as an exponentially saturating function of the nitrogen concentration (with rate constant α_θ),

$$\theta_c(N) = \theta_c^{min} + \Delta\theta_c(1 - e^{-\alpha_\theta N}). \tag{2}$$

Thus, when nitrogen is depleted, the G_1 phase has a minimal length of $\theta_c^{min} - \theta_0$, and the nutrient-independent part of the cell cycle begins at θ_c. In the limit of infinite nitrogen concentrations, however, the G_1 phase is elongated until the phase value $\theta_c^{max} = \theta_c^{min} + \Delta\theta_c$. Since progression in the rest of the cell cycle is nitrogen independent, the length of subsequent segments can be presented by a single parameter, $\Delta\theta_s$, and the phase of cell division is $\theta_{div} = \theta_c(N) + \Delta\theta_s$.

If the cell density at phase θ and time t is denoted as $p(\theta, t)$, its dynamics can be shown in terms of a reaction-diffusion-advection equation,

$$\frac{\partial p}{\partial t} + \frac{\partial}{\partial \theta}[gp] = \frac{\partial}{\partial \theta} D(g) \frac{\partial p}{\partial \theta} - \delta p, \tag{3}$$

where the last term takes into account the losses by the chemostat system with dilution rate δ and the diffusion term $D > 0$ derives from stochastic perturbations (Strogatz 2000; Acebrón et al. 2005). The diffusion coefficient D is assumed to scale proportionally to the square of the maturation velocity $D(g) = \chi g^2$. This quadratic dependence ensures that sharp peaks in the density distribution do not decay when the maturation velocity is zero. In the usual parameterization, however, our model results are not affected by the choice of the diffusion term. To specify the boundary condition, we require that all cells at phase values of θ_{div} and larger divide into n daughter cells with zero phase

$$p(0) = n \int_{\theta_{div}}^{\infty} p(\theta) d\theta. \tag{4}$$

Phase values larger than θ_{div} might occur when the nitrogen concentration decreases from one time step to the next, allowing θ_{div} to decrease below the phase values of some cells. These cells are forced to divide along with all other cells that have reached θ_{div}.

Finally, the model is complemented with a dynamic equation for the nitrogen concentration. We assume that nitrogen uptake occurs only during the G_1 phase, because only here is cell development nitrogen dependent:

$$\dot{N} = \delta(N_i - N) - \nu_{max} \frac{N}{K_N + N} \tilde{P}$$
$$\text{with } \tilde{P} = \int_0^{\theta_{div}} p(\theta, t) d\theta, \tag{5}$$

where N_i is the nitrogen supply concentration, ν_{max} is the maximal nitrogen uptake rate, and $\tilde{P}$ denotes the time-dependent number of cells that are regulated by nitrogen. The total number of phytoplankton cells is given by $P = \int_0^\infty p(\theta, t) d\theta$.

To match the model results to the experimental data, the phase variables must be rescaled to volumes. We assume that the cell volume $V_C(t)$ increases linearly with $\theta(t)$,

$$V_C(t) = V_0(t) + \beta\theta(t), \tag{6}$$

where $V_0(t)$ denotes the volume of a daughter cell immediately after cell division and β measures the increase in cell volume per unit increase in development (i.e.,

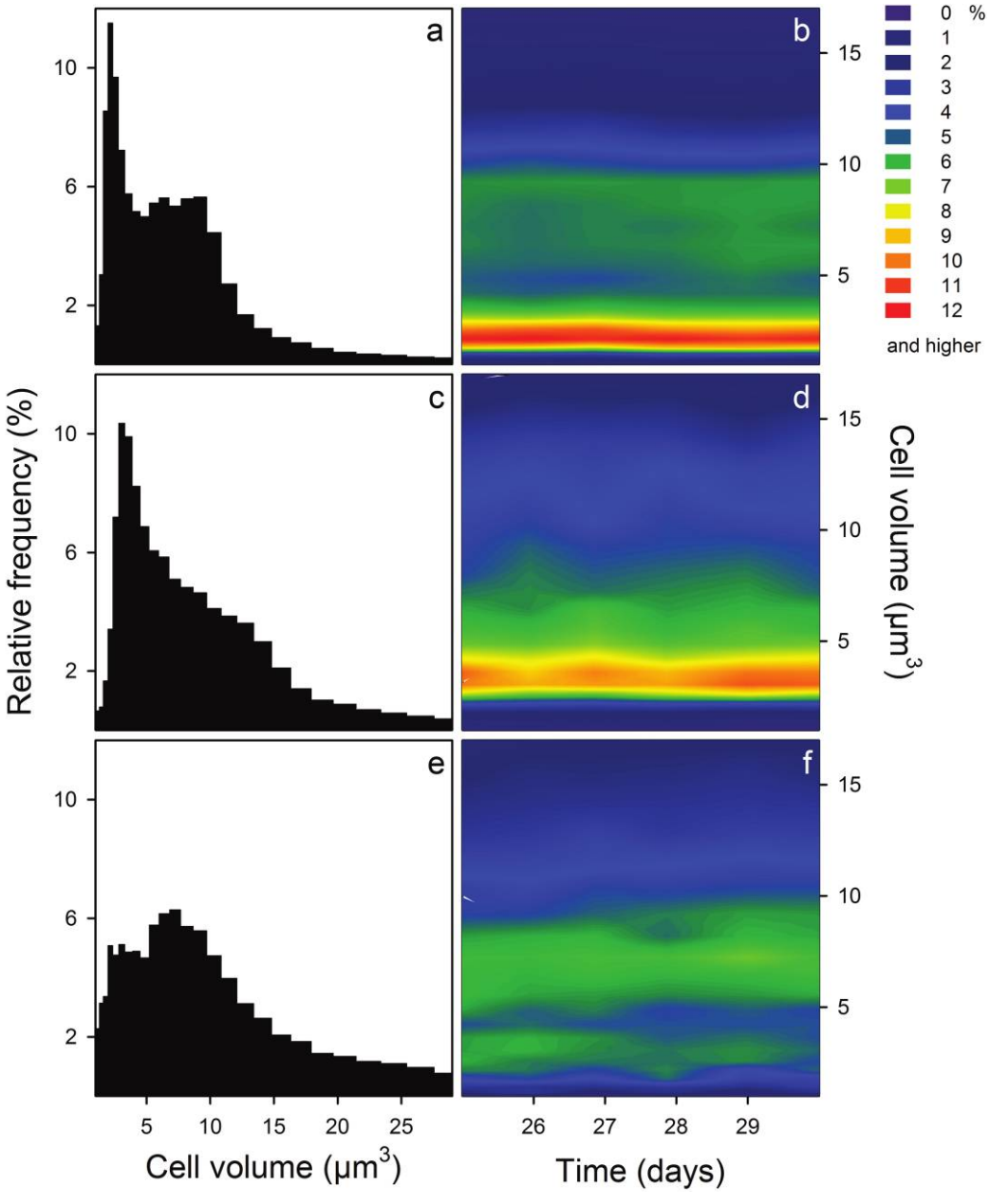

Figure 2: Steady state distributions of cell size in trials 1–3 before perturbations were applied. The corresponding dilution rate was $\delta = 0.48\ \text{day}^{-1}$ in trial 1 (*a*, *b*), $\delta = 0.82\ \text{day}^{-1}$ in trial 2 (*c*, *d*), and $\delta = 1.09\ \text{day}^{-1}$ in trial 3 (*e*, *f*). Panels on the left show the average size distributions over a 5-day sampling interval. Panels on the right show the temporal dynamics of the size distributions within this interval. The colors code the relative frequencies from low (blue) to high (red) values. In each trial, the nitrogen concentration of the supply medium was $N_i = 80\ \mu\text{mol} \cdot \text{L}^{-1}$.

phase). This minimal cell size $V_0(t)$, however, is not constant but depends on the volume and thus the phase θ_{div} of the mother cell during division,

$$V_0(t, i) = \alpha(\theta_{\text{div}} - \theta_{\text{div}}^{\min}) + V_0^{\min}. \tag{7}$$

Here $V_0^{\min}$ is the minimal possible cell volume and $\theta_{\text{div}}^{\min} = \theta_c^{\min} + \Delta\theta_s$ the minimal possible phase of division, both of which are attained in the limit of zero nitrogen concentration $N(t) = 0$.

To fit parameters, we used the differential evolution algorithm of Storn and Price (1997; table B1). We optimized parameters to estimate a combination of K_N, ω, χ,

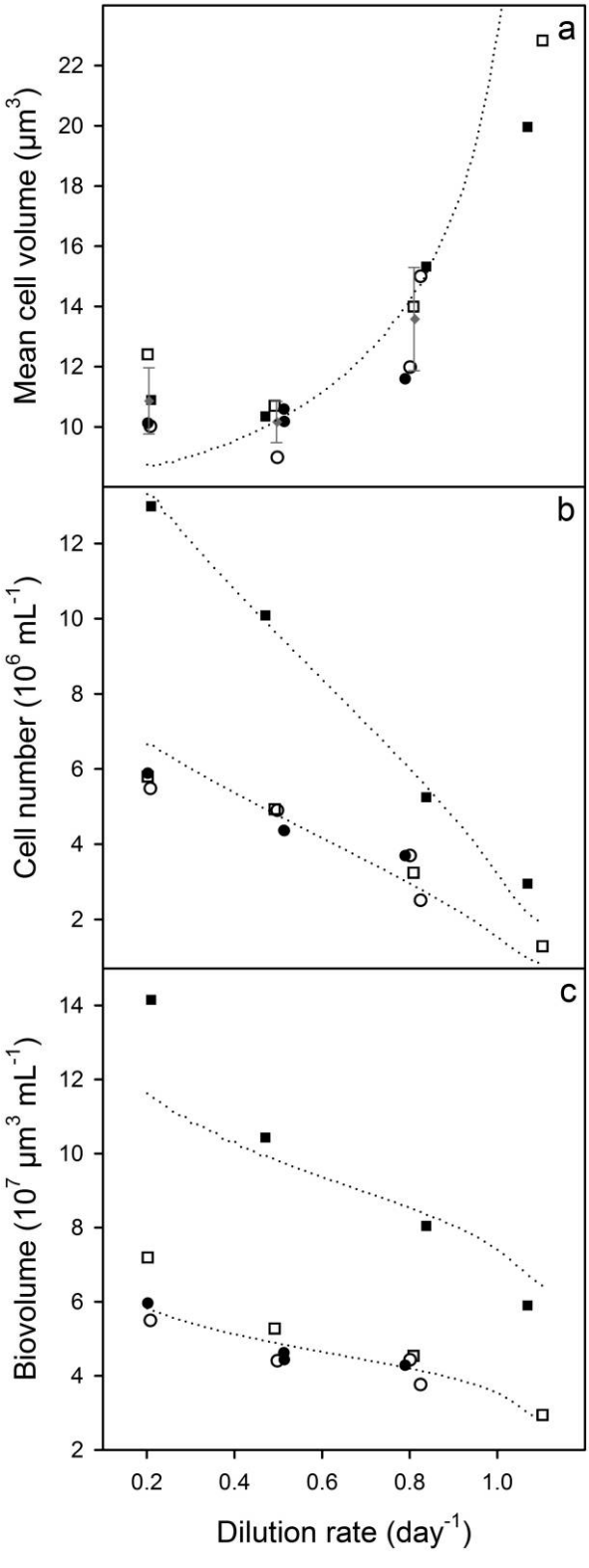

Figure 3: Steady state values of the mean cell volume V_C (*a*), the cell number P (*b*), and the biovolume V_B (*c*) in relation to the dilution rate δ. Squares refer to the first series of experiments (trials 1 and 2, with doubling N_i), and circles refer to the second series of experiments (trials 3–5, with changing δ). Values before perturbation are represented by open symbols and values after the perturbation by filled symbols. In panel *a*, the gray diamonds give the average value of the mean cell volumes and error bars display the simple standard deviation. Dotted lines represent the predicted values obtained from model simulations. The average values of the mean cell volumes were calculated over 15 sampling points at steady state. Values of the dilution rates corresponded to these time intervals.

ν_{max}, α_θ, and $\Delta\theta_c$ that minimizes the mean square deviation of the model outcome to the chemostat cell number in experimental trials 1 and 2, simultaneously. Being fitted for only two experimental trials (trials 1 and 2; see figs. 5 and S1; figs. S1–S4 available online), that parameter set also yielded remarkable agreement between the model outcome and the other experimental trials (trials 3–5; see figs. S2–S4). This verified that the qualitative model results are robust and describe the experimental data obtained under different conditions.

Results

Steady State Conditions

The populations showed characteristic size distributions depending on the chemostat dilution rate at steady state, with broader size distributions at higher dilution rates (fig. 2). Compared to a moderate dilution rate ($\delta = 0.48$ day^{-1}), a higher dilution rate resulted in higher amounts of nitrogen available for the phytoplankton cells, because more nitrogen entered the vessel per unit of time and more cells were washed out of it. As a result, the cells were able to progress faster through the G_1 phase and accumulated less nitrogen in it. This is shown by the size spectra (fig. 2*b*, 2*d*, 2*f*): the frequencies of smaller cells, that is, cells in an early developmental stage, decreased with increasing dilution rates.

The algal cells grew larger at higher dilution rates (fig. 3*a*). While the average value of the mean cell volumes V_C at an average dilution rate of $\delta = 0.2$ day^{-1} and $\delta = 0.50$ day^{-1} were approximately the same ($V_C = 11.14 \pm 0.76$ μm^3, mean $\pm$ SD, and $V_C = 10.14 \pm 0.63$ μm^3, respectively), it clearly increased at $\delta = 0.81$ day^{-1} ($V_C = 13.31 \pm 2.19$ μm^3) and $\delta = 1.09$ day^{-1} ($V_C = 21.53 \pm 2.14$ μm^3). Especially at the highest δ, V_C differed notably from cells at lower δ (being nearly twice as high).

The steady state cell number P^* (fig. 3*b*) and steady state biovolume V_B^* (fig. 3*c*) showed a negative relationship with δ. Doubling the nitrogen supply concentration N_i caused an approximate doubling of P^* and V_B^* (trials 1 and 2, filled squares).

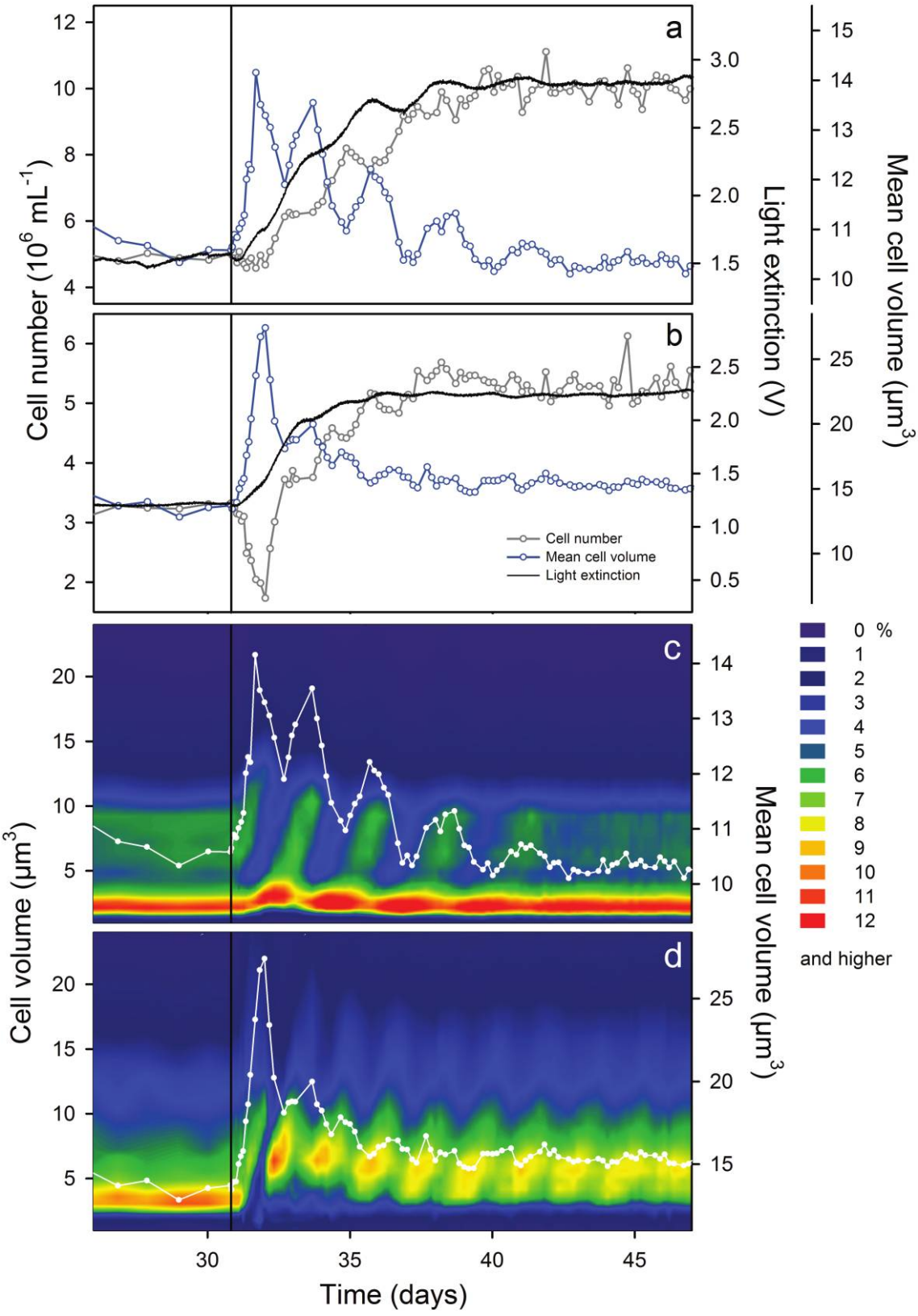

Table 1: Nitrogen concentration of the supply medium N_i, dilution rate δ, and steady state values of cell number P, biovolume V_B, and mean cell volume V_C in the two series of chemostat experiments

	N_i (μmol · L^{-1})			δ (day^{-1})		P (10^6 cells · mL^{-1})		V_B (10^7 μm^3 · mL^{-1})		V_C ± SD (μm^3)		T ± SD (days)
Trial	Before	After	Overall	Before	After	Before	After	Before	After	Before	After	After
1	80	160	.48	.49	.47	4.93	10.09	5.28	10.44	10.7 ± .3	10.3 ± .1	2.67 ± .18
2	80	160	.82	.81	.84	3.24	5.25	4.54	8.05	14.0 ± .6	15.3 ± .4	1.81 ± .09
3	80	80	...	.21	.51	5.49	4.37	5.50	4.63	10.0 ± .5	10.6 ± .4	2.37 ± .18
4	80	80	...	.50	.79	4.90	3.70	4.41	4.29	9.0 ± .3	11.6 ± .3	1.52 ± .25
5	80	80	...	.82	.51	2.51	4.36	3.77	4.44	15.0 ± .4	10.2 ± .4	...

Note: The period length T refers to the oscillations occurring after the chemostat system was perturbated. The overall dilution rate gives the average dilution rate over the total time of an experiment. In the first series of experiments (trials 1 and 2), N_i was doubled from 80 to 160 μmol · L^{-1}, while δ remained constant. In the second series (trials 3–5), δ was altered, while N_i remained constant. The terms "before" and "after" refer to the phases before and after perturbation at $t = 30.8$ days.

Changing the Resource Supply Concentration

In experimental trials 1 and 2, N_i was doubled from 80 to 160 μmol · L^{-1} at $t = 30.80$ days, whereas δ remained constant. This induced transient dynamics displayed by the average population measures (fig. 4*a*, 4*b*) and the population structure (fig. 4*c*, 4*d*). In both trials, the populations responded with more or less pronounced oscillations of P, V_B, V_C, and the size spectra. Damped, small-amplitude oscillations occurred in trial 1 ($\delta = 0.48$ day^{-1}, period length $T = 2.67 \pm 0.18$ days, mean ± SD) and trial 2 ($\delta = 0.82$ day^{-1}, $T = 1.81 \pm 0.09$ days). In both trials, directly after the perturbation, V_C increased by 33% within 0.87 days and by 94% within 1.20 days, respectively. In trial 1, P remained at steady state level for 1.20 days before it started to increase. In trial 2, P first decreased by 47% before it also increased after 1.20 days. V_B evolved in time according to the product of P and V_C. For instance, after the perturbation, V_B in trial 2 remained around the steady state level for 1.20 days because the increase in V_C compensated for the decrease in P.

At the lower dilution rate, oscillations of P, V_B, and V_C were slower and the amplitude was higher (fig. 4*a* and 4*c* vs. 4*b* and 4*d*). The bands in the size spectra showed how the periods of the oscillations are linked to the generation time: a cohort repeatedly consisted of small daughter cells that became large mother cells that divided again into small daughter cells and so on. The increase in cell number was again higher because more cells entered mitosis at the same time compared to less synchronized conditions. This led to more pronounced ups and downs in the transient population dynamics and to longer cycles. After the transient phase, P and V_B approximately doubled due to the doubling of N_i, while V_C converged to the value it maintained before the change or came at least close to it (figs. 3, 4*a*, 4*b*; table 1). The size spectrum resumed the characteristic dilution-rate-related shape it had prior to the change (fig. 4*c*, 4*d*; cf. fig. 2).

The simulation results of the mathematical model are in good agreement with the experimental results, which is illustrated by figure 5 for trial 2. The relative change in the cell number caused by the nutrient doubling is nearly 100%, $\Delta P_{fin}/P_{init} \approx 1$, meaning that the cell number also doubles (fig. 6*a*, gray line and open squares). The first maximal deviation P_{max}/P_{init} (fig. 6*a*, black line and filled squares) equals zero or is negative, because the nutrient doubling leads initially to a drop in the cell number. The absolute value of the first maximal deviation increases with dilution, while $\delta < 0.8$ day^{-1}. However, the model predicts that it should vanish again at large dilution rates when N^* is high so that θ_c in equilibrium approaches the maximal value θ^{max}_c. Reactivity exhibited a similar pattern (see fig. 6*b*, black line and filled circles). The return rate to equilibrium (fig. 6*b*, gray line and open circles) increased with turnover rate while $\delta < 0.8$ day^{-1} and then decreased by approximately 20% at extremely high dilution rates.

Changing the Turnover Rate

In trials 3–5, δ was changed, whereas N_i was kept constant. At $t = 34.00$ days, δ was increased from 0.21 to 0.51 day^{-1} in trial 3 and from 0.50 to 0.79 day^{-1} in trial 4, or reduced from 0.82 to 0.51 day^{-1} in trial 5 (table 1). In analogy to the first series of experiments, changing δ resulted in transient dynamics of average population measures (fig. 7) and

Figure 4: *a*, *b*, Cell number (gray circles), light extinction (curved black line), and mean cell volume (blue circles) in chemostat trials 1 and 2, in which the nitrogen concentration was doubled from $N_i = 80$ μmol · L^{-1} to $N_i = 160$ μmol · L^{-1}. *c*, *d*, The corresponding size spectra and mean cell volume (white line). Dilution rates were $\delta = 0.48$ day^{-1} (*a*, *c*) and $\delta = 0.82$ day^{-1} (*b*, *d*).

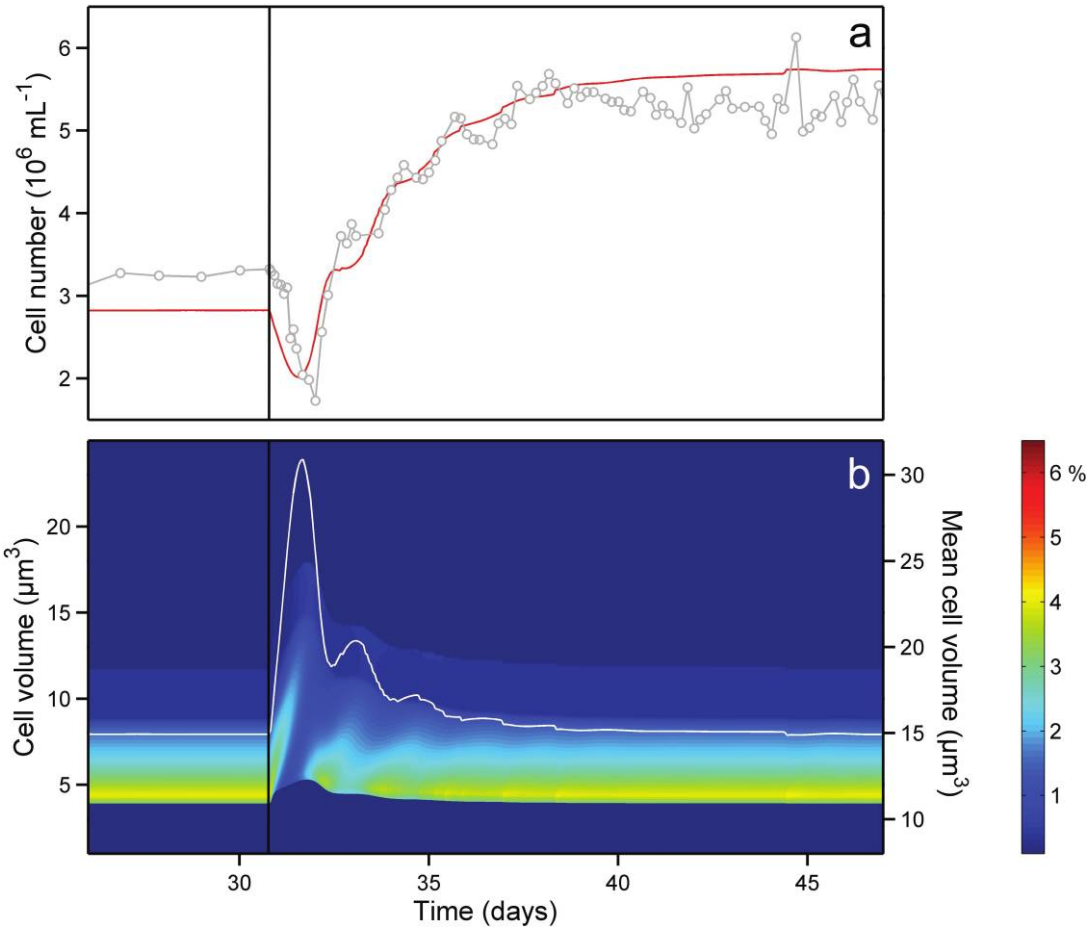

Figure 5: Qualitative agreement between experimental results of trial 2 and model simulations. *a*, The cell number of trial 2 (circles; cf. fig. 4*b*) was well reproduced by simulation of the structured-population model allowing for nitrogen-dependent cell-size variability (red line). *b*, Simulation results also confirmed the dynamic behavior of the size spectrum and the mean cell volume (white line) in trial 2 (cf. fig. 4*d*).

population structure (fig. 8). After a more than twofold increase of δ in trial 3, distinct transient oscillations occurred, whereas the moderate increase of δ in trial 4 resulted in minor oscillations. No oscillations were detected in trial 5.

In trial 3, δ was changed from a comparably low value ($\delta = 0.21$ day^{-1}) to a moderate value ($\delta = 0.51$ day^{-1}). This resulted in damped oscillations of P, V_B, and V_C (fig. 7*a*; $T = 2.37 \pm 0.18$ days). While P and V_B converged downward to the new steady state level (from $5.49 \cdot 10^6$ to $4.37 \cdot 10^6$ cells $\cdot$ mL^{-1} and from $5.50 \cdot 10^7$ to $4.63 \cdot 10^7$ μm^3 $\cdot$ mL^{-1}, respectively), V_C oscillated around approximately the same value it was at before δ was changed ($\approx$10.5 μm^3). The size spectrum oscillated clearly, showing repeating distinct bands from smaller- to larger-sized cells (fig. 8*a*). Finally, the size spectrum slowly converged to the shape that is characteristic for a dilution rate of about $\delta = 0.5$ day^{-1} (cf. fig. 2*a*).

In trial 4, δ was changed from a moderate value ($\delta = 0.50$ day^{-1}) to a comparatively high value ($\delta = 0.79$ day^{-1}). Although δ was increased, the average population measures showed nearly no oscillations (P, V_C) or only minor oscillations (V_B; fig. 7*b*; $T = 1.52 \pm 0.25$ days). Variables P and V_B converged downward to the new steady state level (from $4.90 \cdot 10^6$ to $3.70 \cdot 10^6$ cells $\cdot$ mL^{-1} and from $4.41 \cdot 10^7$ to $4.29 \cdot 10^7$ μm^3 $\cdot$ mL^{-1}, respectively), while V_C increased from 9.0 ± 0.3 to 11.6 ± 0.3 μm^3. The size spectrum showed only minor oscillations and finally converged to the shape that is characteristic for a dilution rate of about $\delta = 0.8$ day^{-1} (fig. 8*b*).

Trial 5 represents the opposite of trial 4: δ was changed from a comparably high value ($\delta = 0.82$ day^{-1}) to a mod-

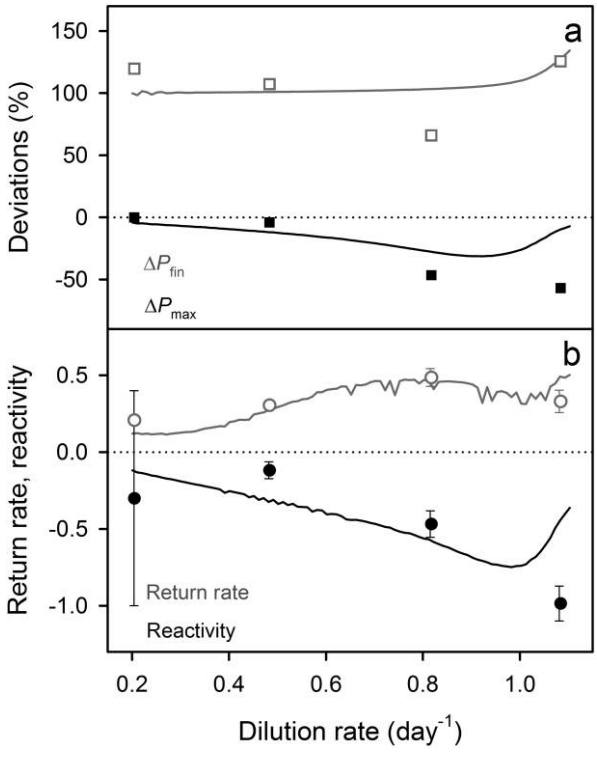

Figure 6: Transient indexes calculated in the numerical model (solid lines) and based on the experimental results (data points). *a*, The first maximal deviation ΔP_{max} (black line) and the final deviation ΔP_{fin} plotted as percent of the initial cell number (gray line). *b*, Reactivity (black line) and return rate to equilibrium (gray line).

erate value ($\delta = 0.51$ day^{-1}). The average population measures (fig. 7*c*) as well as the size spectrum (fig. 8*c*) indicated that oscillations were not strongly evident. The oscillations occurring after $t = 40.6$ days are due to a malfunction of the pump that perturbed the population structure. Until that point in time, P, V_B, and V_C smoothly transitioned to values characteristic for a dilution rate of about $\delta = 0.5$ day^{-1} (from $2.51 \cdot 10^6$ to $4.36 \cdot 10^6$ cells $\cdot$ mL^{-1}, from $3.77 \cdot 10^7$ to $4.44 \cdot 10^7$ μm^3 $\cdot$ mL^{-1}, and from 15.0 ± 0.3 to 10.2 ± 0.4 μm^3, respectively; fig. 6*b*).

Discussion

Population dynamics are determined by numerous biotic and abiotic factors that differently impact the developmental stages of individuals within a population. Growth and death rates originating from the interaction between organisms and their environment are unequally distributed over an organism's life cycle. Hence, the environment defines the steady state shape of a population's stage distribution. In a constant environment and in the absence of processes that lead to stable limit cycles or chaotic attractors, populations will adjust to the prevailing conditions and finally show a characteristic stage distribution, as was found in our experiments (fig. 2).

Steady State and Cell Size

Resource shortage is one of the most important factors influencing organismal processes. In our case, nitrogen was the essential resource limiting the maturation velocity at which the *Chlorella* cells progressed through the first stage (G_1 phase) of their life cycle. This led to the hypothesis that the number of cells inside and outside of the G_1 phase could be predicted from the availability of nitrogen. Based on the simplistic but reasonable assumption that developmental progression is correlated with cell size (early developmental stages are represented by small cell sizes and vice versa; cf. Massie et al. [2010]), our empirical results accurately matched this prediction. The frequency distribution of cell volumes was consistently closely related to the chemostat's dilution rate δ at steady state (e.g., figs. 2, 4, 8). While low and moderate values of δ resulted in the dominance of small cells ($\delta = 0.49$ day^{-1} in fig. 2*a*, 2*b* and $\delta = 0.82$ day^{-1} in fig. 2*c*, 2*d*), distinctly fewer cells accumulated in this size interval at a high value of δ ($\delta = 1.09$ day^{-1} in fig. 2*e*, 2*f*). That is, cells progressed more slowly through their life cycle at low δ because the low ambient nitrogen concentration hampered transition from the G_1 phase to the S phase. The resulting formation of a cohort (principally consisting of small daughter cells) and the cohort's size are directly related to the degree of synchrony (Massie et al. 2010). As well as being correlated with developmental progression, the cell size also varied with the availability of nitrogen determined by δ. The mean cell volume at steady state clearly increased with increasing δ (fig. 3*a*), supporting the model assumption that cells increase in size when taking up surplus nitrogen.

Response to Perturbations

Constant environmental conditions are rare in natural systems and are always a matter of scale. Thus, most natural populations experience an environment that is characterized by fluctuations and transitions. Here we experimentally imposed press perturbations of environmental conditions by altering the nitrogen supply concentration, N_i, and δ, that is, the parameters reflecting the fundamental growth conditions of natural populations (resource supply and mortality). In four of the five trials, oscillations in cell number P, biovolume V_B, mean cell volume V_C, and size spectra characterized the transient behavior. Independent of which parameter was altered, the oscillations showed larger amplitudes and longer periods the lower δ was before the conditions changed. This originates from the

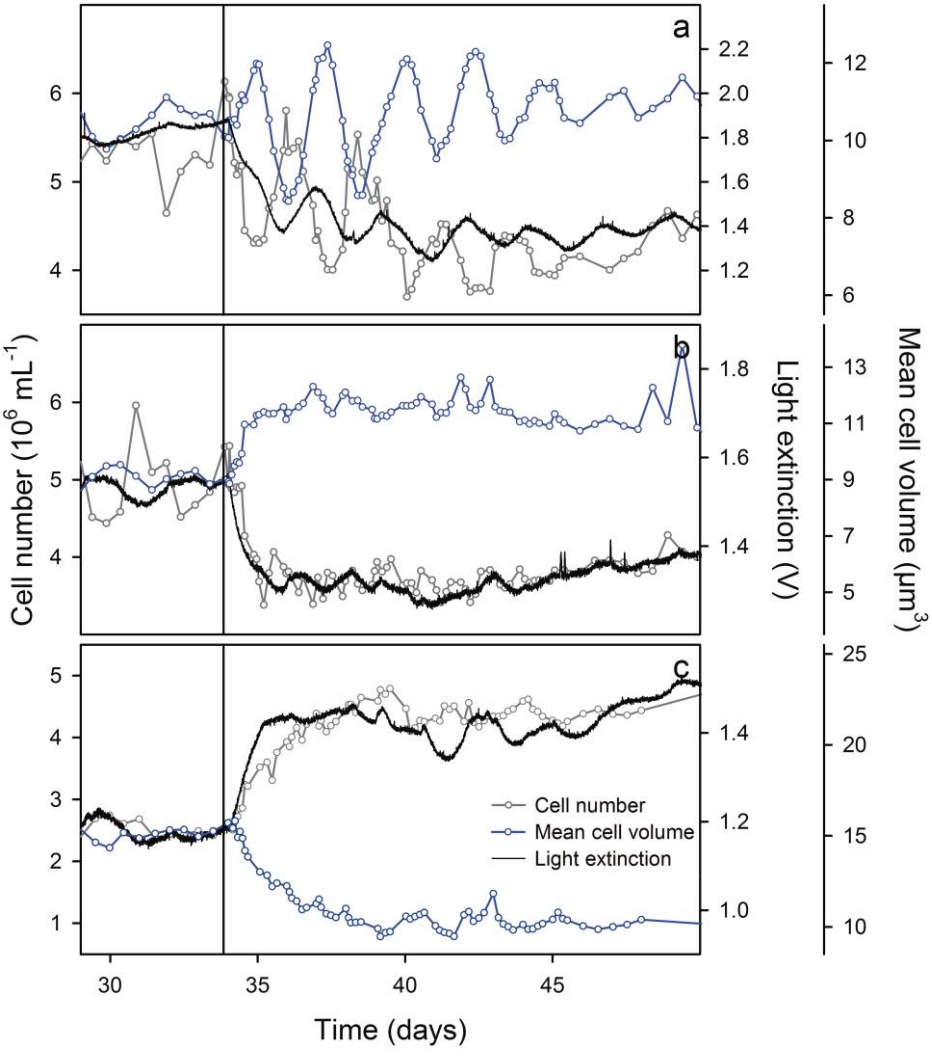

Figure 7: Cell number (gray circles), light extinction (black ragged line), and mean cell volume (blue circles) in chemostat trials 3–5, in which the dilution rate δ was changed from (*a*) $\delta = 0.21$ day^{-1} to $\delta = 0.51$ day^{-1}, (*b*) $\delta = 0.50$ day^{-1} to $\delta = 0.79$ day^{-1}, and (*c*) $\delta = 0.82$ day^{-1} to $\delta = 0.51$ day^{-1}, respectively. The nitrogen concentration of the supply medium was constant at $N_i = 80$ μmol $\cdot$ L^{-1}.

steady state results described above. The frequency distributions of the size spectra revealed that in trial 1 ($\delta = 0.48$ day^{-1}; fig. 4*a*, 4*c*), more cells accumulated in the small size range than in trial 2 ($\delta = 0.82$ day^{-1}; fig. 4*b*, 4*d*) and strong oscillations resulted from a large cohort within the population. The high degree of synchrony arose from the strong limitation due to low δ. Thus, the oscillations in trial 1 were significantly stronger than in trial 2, since the traveling cohort in trial 1 proportionally consisted of more cells.

The dependence of the population-dynamical response on the original environmental conditions becomes even clearer when comparing trials 3 and 5 in the second series of experiments. Although experiencing almost identical environmental conditions ($\delta \approx 0.5$ day^{-1}), the oscillations were stronger when coming from $\delta = 0.21$ day^{-1} (figs. 7*a*, 8*a*) than when coming from $\delta = 0.82$ day^{-1} (figs. 7*c*, 8*c*). This is again explicable by the stronger preperturbation resource limitation and thus greater synchronization at lower δ. In addition, although the dilution rate in trial 3 was increased by the same absolute value as in trial 4 ($\Delta\delta \approx 0.30$ day^{-1}), the oscillations were distinctly stronger in trial 3, since δ was initially lower.

Resource-Dependent Cell-Size Variability

In addition to the transient oscillations arising from demographic processes, we observed the counterintuitive be-

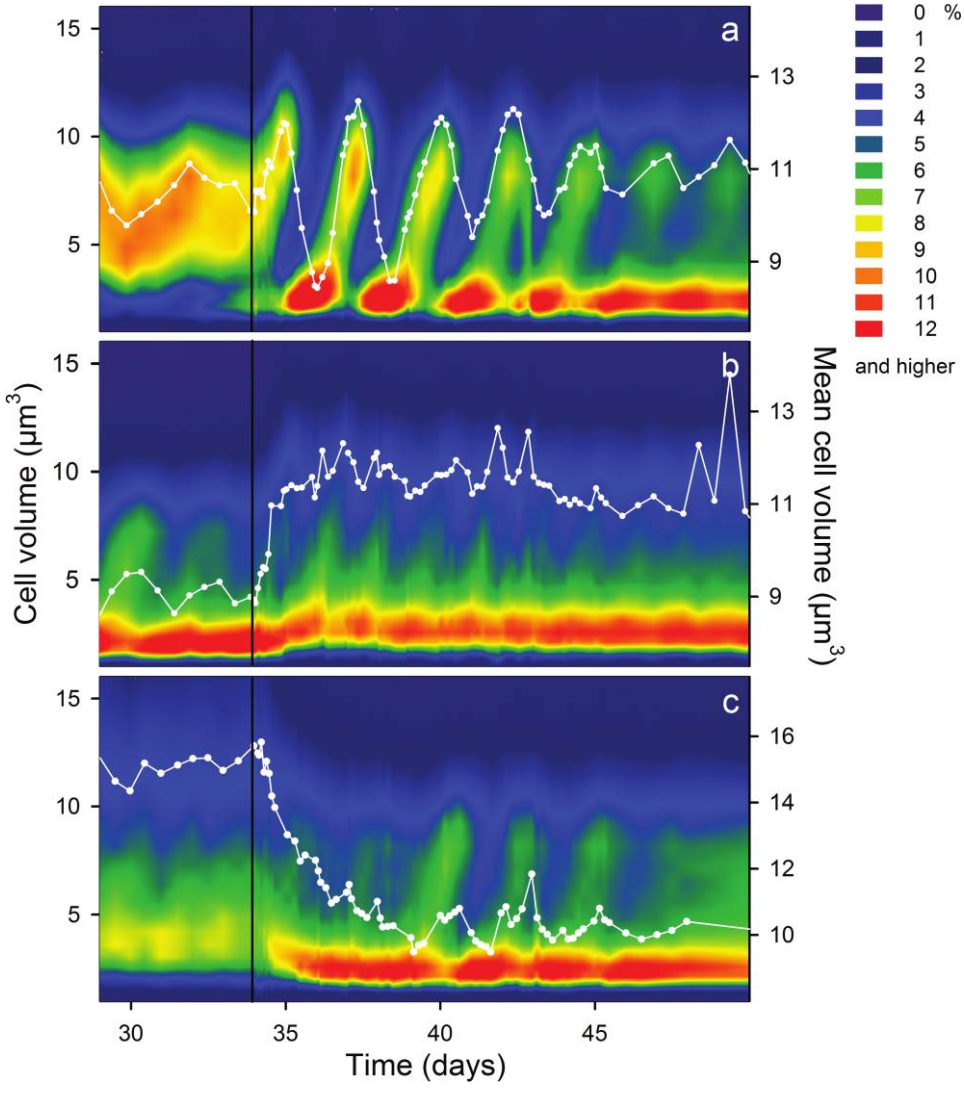

Figure 8: Size distribution and mean cell volume (white circles) of chemostat trials 3–5. Dilution rates and the nitrogen concentration of the supply medium are as in figure 7.

havior of P when N_i was doubled. Populations are supposed to grow when resource concentrations ameliorate. This was true for V_B, which immediately increased toward the new steady state value defined by N_i (determining the carrying capacity), in accordance with simple, nonstructured models. Surprisingly, however, after doubling N_i in trial 2, P decreased considerably to about 50% of the previous steady state value (fig. 4*b*) and increased again after 1.2 days. In contrast, the mean cell volume escalated to twice its value prior to the change in N_i. This supports our hypothesis that V_C increases when surplus nitrogen is available. As N_i was doubled, more nitrogen entered the system and the cells were able to take up the surplus nitrogen. Thus, the majority of the cells grew in size but did not proliferate immediately. That is, the time necessary to complete one cell cycle was prolonged compared to the previous steady state conditions, causing a decline in P due to the washout by δ. This effect was less pronounced in trial 1, since δ was lower and comparably fewer nutrients per unit time entered the chemostat. As a result, P merely increased in size by about 30% and the cell cycle was not substantially prolonged.

An alternative explanation for the cells growing larger might be the formation of more rather than larger daughter cells. However, we reject this, because if more daughter cells had been formed, the cell size of the daughter cells should have been at a fixed starting value. That is, the bands of the size spectra should have always started at a

minimum cell volume V_0 of approximately 3 μm^3. However, this was not consistent with our observations. In fact, the cell volume of the first generation of daughter cells occurring directly after N_i was doubled ($V_0 \approx 6$ μm^3; fig. 4*d*). The whole band was clearly shifted toward higher cell volumes. This shift lasted for another generation before V_0 converged to the original value of 3 μm^3, indicating that the released daughter cells had again started at a volume of $V_0 = 3$ μm^3 due to the increase in P.

In addition to the different experimental findings complementing one another, the reliability of the hypothesized mechanism is strongly supported by the results of our simulation model. By adding nitrogen-dependent cell-size variability to the model by Massie et al. (2010), we were able to imitate the two distinct dynamical features in the time series of trial 2: the temporary decrease of P (fig. 5*a*) and the increasing size of the daughter cells (fig. 5*b*) directly after the doubling of N_i. We also ran simulations with an alternative model that accounted for division into more rather than larger daughter cells. The population dynamics were qualitatively the same, but we rejected this mechanism since it failed to explain the occurrence of larger daughter cells as observed in our experiments. That is, we explicitly accounted for two reasonable mechanisms leading to a lagged growth response instead of just implementing a time lag into the functional response equation. Models solely describing overall measures of population dynamics would not adequately reflect the processes leading to the dynamics we observed and would also fail to explain the discrepancy in the behavior of P, V_B, and V_C after N_i was doubled.

Implications for Natural Populations

In ecological studies, microcosm experiments play an important role in examining fundamental aspects of population dynamics and stability (Jessup et al. 2004). Chemostat cultures are generally regarded as idealizations of natural populations. Chemostats are characterized as open systems and allow for the investigation of continuous processes as found in nature: resource inputs and outputs are analogous to the continuous turnover of nutrients/resources; and washout by dilution is analogous to a mortality being independent of developmental stages and population density (Novick and Szilard 1950; Smith and Waltman 1995). By altering N_i and δ, we applied press perturbations that correspond to resource enrichment or eutrophication and changes in turnover and mortality. Resource enrichment is a process causing problems in various ecological systems. It is mostly caused by anthropogenic land use and therefore impacts populations and habitats on a global scale (Smith et al. 1999; Millennium Ecosystem Assessment 2005). Changes in the chemostats' dilution rate can be directly interpreted as changes in the turnover rate in a lake ecosystem due to an altered runoff. This corresponds well to the changes in the dilution rate: if more water enters a lake, the turnover rate is increased and vice versa. Moreover, runoff generally involves the load with nutrients, which again affects the system's resource availability. However, one can also regard changes in the dilution rate more generally as changes in mortality (Smith and Waltman 1995). Fishing, for instance, can be discussed in terms of a density-independent mortality rate: individuals are removed from a population regardless of the stock size. Hence, fishing has a direct effect as it alters the population structure and an indirect effect as it increases the per capita resource availability. It was shown that fishing altered the population structure of fish stocks, mainly by truncating the size and age distributions (Hutchings and Reynolds 2004; Longhurst 2006), thereby increasing the population-dynamical variability (Hsieh et al. 2006; Anderson et al. 2008). In principle, this agrees with the dynamical behavior of our experimental *Chlorella* populations: altering the population structure led to changes in the specific cohort properties, thus generating fluctuations that increased variability. Due to the general approach of chemostat experiments, the results obtained from our microcosms are of relevance for most natural populations, regardless of the kind of habitat they occupy.

Transient dynamics become even more complex when mechanisms other than those related to the shape of the stage distribution come into play. In our study, the *Chlorella* population stopped growing when the environmental conditions ameliorated (i.e., with the doubling of N_i). Thus, surplus amounts rather than a shortage of resources had a temporarily negative effect on the density of the population. The use of surplus resources may result in diverse life-history strategies showing strong variation in size and age at maturity as well as in size and number of offspring. For example, an organism might reproduce faster at a younger age and smaller size. Or, as is the case for *Chlorella vulgaris* in our study, it may increase in size, reproduce later, and produce larger offspring. Under the conditions given in our chemostat experiments, we assume that *C. vulgaris* increases its individual size with increasing nitrogen levels until the daughter cells reach a specific maximum size (≈ 6 μm^3). Only when the nitrogen availability further increases do the mother cells (still increasing in size) produce more than four daughter cells (or possibly build colonies). Figure B2 in appendix B (figs. A1–A5 and B1, B2 available online) provides a schematic description of this life-history strategy.

This response mechanism is beneficial at higher resource input. In this case, the offspring is larger in size and has a better constitution when released from the mother cells. But this mechanism is also reasonable when the population

experiences losses due to predation. In this case, the per capita resource availability increases and the cells are able to grow larger. A larger body size may reduce predation, especially when exceeding a critical size too large for gape-limited predators. In both cases, the growth of *C. vulgaris* cells is triggered by resource availability. We assume that using a single mechanism in both situations may have evolved due to the fact that *C. vulgaris* has no sensory systems to detect predators. In either case, growing larger seems to be a reasonable way to increase individual fitness (e.g., Werner and Gilliam 1984; Clutton-Brock 1988; Sogard 1997; Berube et al. 1999; Gaillard et al. 2000; Beauplet and Guinet 2007).

Many organisms follow the larger and size-delayed reproduction strategy when experiencing surplus resources or predation. In this respect, the trigger to increase in size can be direct as an avoidance strategy against size-selective predators (Crowl and Covich 1990; Abrams and Rowe 1996). However, it can also be indirect as the result of an ameliorated resource availability when a predator is present (Skelly and Werner 1990; Werner 1991; Abrams and Rowe 1996).

In this study, we explored the dynamic responses of structured populations to press perturbations. Moreover, pulse perturbations can also impact the population structure and therefore the dynamics, depending on the amplitude and frequency by which the perturbations occur. Rare or single pulses may result in similar transient dynamics as caused by press perturbations. However, a single-pulse perturbation will allow a population to return to the preperturbation state. When pulses occur more frequently, the response behavior might range from simple, linear changes of the population density to rather complex dynamics, such as cyclic and chaotic behaviors (Nisbet and Gurney 1976; Holt 2008).

Our results show that predicting transient responses of population dynamics to press perturbations even for seemingly simple single-celled organisms can require explicit modeling of stage structure. Our chemostat populations responded highly sensitively: even minor perturbations caused changes in the population structure that altered population dynamics. Whether this holds for the dynamics of natural populations will crucially depend on other density-dependent processes, for example, how the population is embedded in an interaction web.

Acknowledgments

This work was supported by the German Science Foundation (DFG; project number BL 772/1–1), the Volkswagen Foundation, and the Swiss National Science Foundation (SNF). We thank O. L. Petchey for helpful comments on a previous version of the manuscript and appreciate the helpful comments of two anonymous reviewers and the editors.

Literature Cited

Abrams, P. A., and L. Rowe. 1996. The effects of predation on the age and size of maturity of prey. Evolution 50:1052–1061.

Acebrón, J. A., L. L. Bonilla, C. J. Pérez Vicente, F. Ritort, and R. Spigler. 2005. The Kuramoto model: a simple paradigm for synchronization phenomena. Reviews of Modern Physics 77:137–185.

Anderson, C. N. K., C.-H. Hsieh, S. A. Sandin, R. Hewitt, A. Hollowed, J. Beddington, R. M. May, and G. Sugihara. 2008. Why fishing magnifies fluctuations in fish abundance. Nature 452:835–839.

Arino, O., and M. Kimmel. 1993. Comparison of approaches to modeling of cell population dynamics. Journal on Applied Mathematics 53:1480–1504.

Balagaddé, F. K., L. You, C. L. Hansen, F. H. Arnold, and S. R. Quake. 2005. Long-term monitoring of bacteria undergoing programmed population control in a microchemostat. Science 309:137–140.

Beauplet, G., and C. Guinet. 2007. Phenotypic determinants of individual fitness in female fur seals: larger is better. Proceedings of the Royal Society B: Biological Sciences 274:1877–1883.

Benton, T. G., T. C. Cameron, and A. Grant. 2004. Population responses to perturbations: predictions and responses from laboratory mite populations. Journal of Animal Ecology 73:983–995.

Berube, C. H., M. Festa-Bianchet, and J. T. Jorgenson. 1999. Individual differences, longevity, and reproductive senescence in bighorn ewes. Ecology 80:2555–2565.

Bierzychudek, P. 1999. Looking backwards: assessing the projections of a transition matrix model. Ecological Applications 9:1278–1287.

Cameron, T. C., and T. G. Benton. 2004. Stage-structured harvesting and its effects: an empirical investigation using soil mites. Journal of Animal Ecology 73:996–1006.

Caperon, J., and J. Meyer. 1972. Nitrogen-limited growth of marine phytoplankton. I. Changes in population characteristics with steady-state growth rate. Deep Sea Research and Oceanographic Abstracts 19:601–618.

Caswell, H. 2000. Matrix population models: construction, analysis and interpretation. Sinauer, Sunderland, MA.

Cattadori, I. M., D. T. Haydon, and P. J. Hudson. 2005. Parasites and climate synchronize red grouse populations. Nature 433:737–741.

Cipollina, C., M. Vai, D. Porro, and C. Hatzis. 2007. Towards understanding of the complex structure of growing yeast populations. Journal of Biotechnology 128:393–402.

Clutton-Brock, T. H. 1988. Reproductive success: studies of individual variation in contrasting breeding systems. Vol. 1. University of Chicago Press, Chicago.

Clutton-Brock, T. H., and T. Coulson. 2002. Comparative ungulate dynamics: the devil is in the detail. Philosophical Transactions of the Royal Society B: Biological Sciences 357:1285–1298.

Costantino, R. F., J. M. Cushing, B. Dennis, and R. A. Desharnais. 1995. Experimentally induced transitions in the dynamic behaviour of insect populations. Nature 375:227–230.

Coulson, T. N., F. Guinness, J. Pemberton, and T. H. Clutton-Brock. 2004. The demographic consequences of releasing a population of red deer from culling. Ecology 85:411–422.

Crowl, T. A., and A. P. Covich. 1990. Predator-induced life-history shifts in a fresh-water snail. Science 247:949–951.

Dennis, B., R. A. Desharnais, J. M. Cushing, S. M. Henson, and R.

F. Costantino. 2001. Estimating chaos and complex dynamics in an insect population. Ecological Monographs 71:277–303.
Dortch, Q., J. R. Clayton, and S. S. Thoresen. 1984. Species differences in accumulation of nitrogen pools in phytoplankton. Marine Biology 250:237–250.
Gaillard, J. M., M. Festa-Bianchet, N. Yoccoz, A. Loison, and C. Toigo. 2000. Temporal variation in fitness components and population dynamics of large herbivores. Annual Review of Ecology and Systematics 31:367–393.
Gould, A. R., N. P. Everett, T. L. Wang, and H. E. Street. 1981. Studies on the control of the cell cycle in cultured plant cells. I. Effects of nutrient limitation and nutrient starvation. Protoplasma 106:1–13.
Guillard, R. R. L., and C. J. Lorenzen. 1972. Yellow-green algae with chlorophyllide *c*. Journal of Phycology 8:10–14.
Haddad, N. M., D. Tilman, and J. M. H. Knops. 2002. Long-term oscillations in grassland productivity induced by drought. Ecology Letters 5:110–120.
Hastings, A. 2004. Transients: the key to long-term ecological understanding? Trends in Ecology and Evolution 19:39–45.
Hatzis, C., and D. Porro. 2006. Morphologically-structured models of growing budding yeast populations. Journal of Biotechnology 124:420–438.
Henson, S. M., J. M. Cushing, R. F. Costantino, B. Dennis, and R. A. Desharnais. 1998. Phase switching in population cycles. Proceedings of the Royal Society B: Biological Sciences 265:2229–2234.
Holt, R. D. 2008. Theoretical perspectives on resource pulses. Ecology 89:671–681.
Hsieh, C.-H., C. S. Reiss, J. R. Hunter, J. R. Beddington, R. M. May, and G. Sugihara. 2006. Fishing elevates variability in the abundance of exploited species. Nature 443:859–862.
Humphrey, T., and G. Brooks. 2010. Cell cycle control: mechanisms and protocols. Humana, Totowa, NJ.
Hutchings, J. A., and J. D. Reynolds. 2004. Marine fish population collapses: consequences for recovery and extinction risk. BioScience 54:297–309.
Jenouvrier, S., C. Barbraud, and H. Weimerskirch. 2005. Long-term contrasted responses to climate of two Antarctic seabird species. Ecology 86:2889–2903.
Jeppesen, E., B. Kronvang, M. Meerhoff, M. Søndergaard, K. M. Hansen, H. E. Andersen, T. L. Lauridsen, et al. 2007. Climate change effects on runoff, catchment phosphorus loading and lake ecological state, and potential adaptations. Journal of Environmental Quality 38:1930–1941.
Jessup, C. M., R. Kassen, S. E. Forde, B. Kerr, A. Buckling, P. B. Rainey, and B. J. M. Bohannan. 2004. Big questions, small worlds: microbial model systems in ecology. Trends in Ecology and Evolution 19:189–197.
Kendall, B. E., C. J. Briggs, W. W. Murdoch, and P. Turchin. 1999. Why do populations cycle? a synthesis of statistical and mechanistic modeling approaches. Ecology 80:1789–1805.
Longhurst, A. 2006. The sustainability myth. Fisheries Research 81: 107–112.
Manderson, J. P. 2008. The spatial scale of phase synchrony in winter flounder (*Pseudopleuronectes americanus*) production increased among southern New England nurseries in the 1990s. Canadian Journal of Fisheries and Aquatic Sciences 65:340–351.
Massie, T. M., B. Blasius, G. Weithoff, U. Gaedke, and G. F. Fussmann. 2010. Cycles, phase synchronization, and entrainment in single-species phytoplankton populations. Proceedings of the National Academy of Sciences of the USA 107:4236–4241.
Millennium Ecosystem Assessment. 2005. Ecosystems and human well-being: synthesis. Vol. 5. Island, Washington, DC.
Morgan, D. O. 2007. The cell cycle: principles of control. New Science, London.
Mueller, L. D., and A. Joshi. 2000. Stability in model populations. Princeton University Press, Princeton, NJ.
Neubert, M. G., and H. Caswell. 1997. Alternatives to resilience for measuring the responses of ecological systems to perturbations. Ecology 78:653–665.
Nisbet, R. M., and W. S. C. Gurney. 1976. Population dynamics in a periodically varying environment. Journal of Theoretical Biology 56:459–475.
Novick, A., and L. Szilard. 1950. Description of the chemostat. Science 112:715–716.
Olson, R. J., and S. W. Chisholm. 1986. Effects of light and nitrogen limitation on the cell-cycle of the dinoflagellate *Amphidinium carteri*. Journal of Plankton Research 8:785–793.
Olson, R. J., D. Vaulot, and S. W. Chisholm. 1986. Effects of environmental stresses on the cell cycle of two marine phytoplankton species. Plant Physiology 80:918–925.
Parmesan, C., and G. Yohe. 2003. A globally coherent fingerprint of climate change impacts across natural systems. Nature 421:37–42.
Pascual, M., and H. Caswell. 1997. From the cell cycle to population cycles in phytoplankton-nutrient interactions. Ecology 78:897–912.
Quayle, W. C., L. S. Peck, H. Peat, J. C. Ellis-Evans, and P. R. Harrigan. 2002. Extreme responses to climate change in Antarctic lakes. Science 295:645.
Radchuk, V., C. Turlure, and N. Schtickzelle. 2012. Each life stage matters: the importance of assessing the response to climate change over the complete life cycle in butterflies. Journal of Animal Ecology, doi:10.1111/j.1365-2656.2012.02029.x.
Rhee, G.-Y. 1978. Effects of N : P atomic ratios and nitrate limitation on algal growth, cell composition, and nitrate uptake. Limnology and Oceanography 23:10–25.
Skelly, D. K., and E. E. Werner. 1990. Behavioral and life-historical responses of larval American toads to an odonate predator. Ecology 71:2313–2322.
Smith, H. L., and P. Waltman. 1995. The theory of the chemostat: dynamics of microbial competition. Cambridge University Press, Cambridge.
Smith, V. H., G. D. Tilman, and J. C. Nekola. 1999. Eutrophication: impacts of excess nutrient inputs on freshwater, marine, and terrestrial ecosystems. Environmental Pollution 100:179–196.
Sogard, S. M. 1997. Size-selective mortality in the juvenile stage of teleost fishes: a review. Bulletin of Marine Science 60:1129–1157.
Storn, R., and K. Price. 1997. Differential evolution: a simple and efficient heuristic for global optimization over continuous spaces. Journal of Global Optimization 11:341–359.
Strogatz, S. H. 2000. From Kuramoto to Crawford: exploring the onset of synchronization in populations of coupled oscillators. Physica D: Nonlinear Phenomena 143:1–20.
Tuljapurkar, S., and H. Caswell. 1997. Structured-population models in marine, terrestrial, and freshwater systems. Springer, Berlin.
Vaulot, D., R. J. Olson, S. Merkel, and S. W. Chisholm. 1987. Cell-cycle response to nutrient starvation in two phytoplankton species, *Thalassiosira weissflogii* and *Hymenomonas carterae*. Marine Biology 95:625–630.
Walther, G.-R., E. Post, P. Convey, A. Menzel, C. Parmesan, T. J. C.

Beebee, J.-M. Fromentin, O. Hoegh-Guldberg, and F. Bairlein. 2002. Ecological responses to recent climate change. Nature 416: 389–395.

Walz, N., T. Hintze, and R. Rusche. 1997. Algae and rotifer turbidostats: studies on stability of live feed cultures. Hydrobiologia 358:127–132.

Werner, E. E. 1991. Nonlethal effects of a predator on competitive interactions between two anuran larvae. Ecology 72:1709–1720.

Werner, E. E., and J. F. Gilliam. 1984. The ontogenetic niche and species interactions in size-structured populations. Annual Review of Ecology and Systematics 15:393–425.

Associate Editor: Wolf M. Mooij
Editor: Troy Day

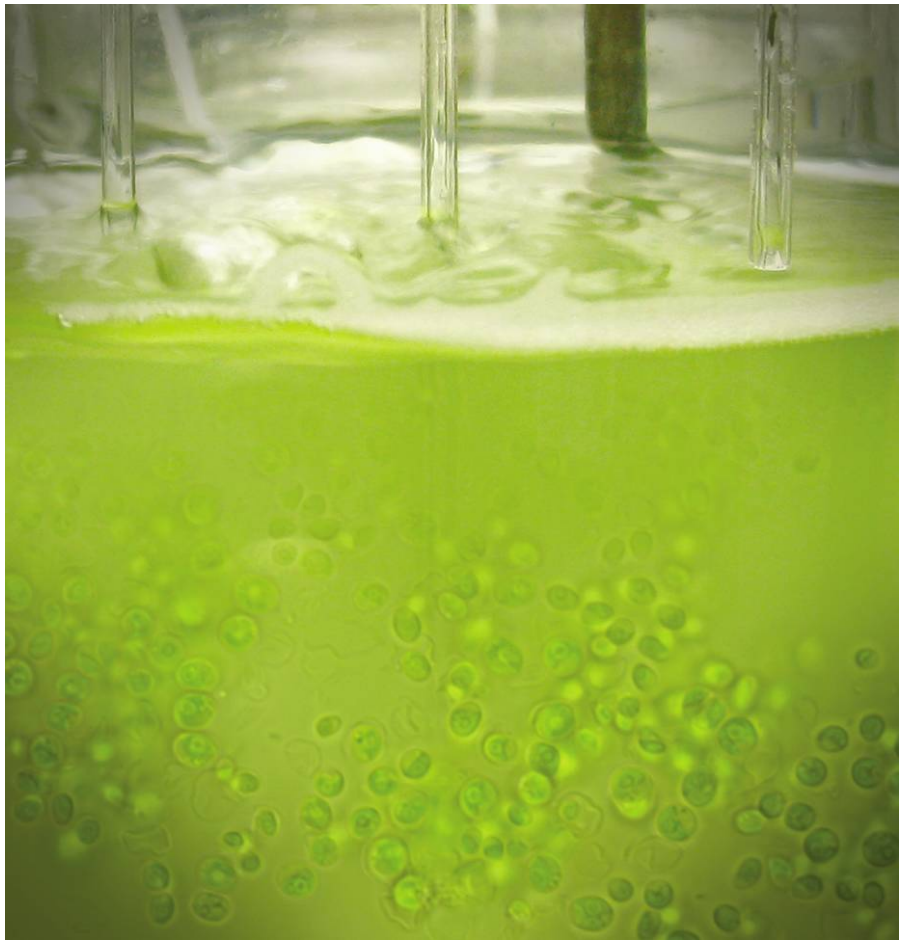

Detail of an experimental chemostat vessel with magnified (× 1,000) cells of the cultured model organism, the green alga *Chlorella vulgaris*. Variable sizes reflect different developmental stages, from small daughter cells to rather large mother cells. Glass tubes above the water level are used for sampling, to supply fresh medium and sterile air, and for adjusting the experimental volume. Photograph by Thomas M. Massie.